Modeling Polybenzimidazole/Phosphoric Acid Membrane Behaviour in a HTPEM Fuel Cell

C. Siegel*[1,2], G. Bandlamudi[1,2] and A. Heinzel[1,2]
[1]Zentrum für BrennstoffzellenTechnik (ZBT) gGmbH, Duisburg, Germany
[2]University of Duisburg-Essen, Institut für Energie- und Umweltverfahrenstechnik, Germany
*Corresponding author: Zentrum für BrennstoffzellenTechnik (ZBT) gGmbH, Carl-Benz-Straße 201, D-47057 Duisburg, Germany, c.siegel@zbt-duisburg.de

Abstract: Phosphoric acid (H_3PO_4) doped polybenzimidazole (PBI) membranes are commonly used in today's high-temperature polymer-electrolyte-membrane (HTPEM) fuel cell technology. COMSOL Multiphysics is used to model and simulate the three-dimensional, single-phase, non-isothermal overall cell behaviour (e.g., species mass fraction distribution, solid-phase and fluid-(gas)-phase temperature distribution) at different operating points. The sol-gel PBI/H_3PO_4 membrane behaviour is modeled using an Arrhenius approach, accounting for the activation energy and the membrane doping level. Simulation results are compared to experimental investigations performed at the Zentrum für BrennstoffzellenTechnik (ZBT) gGmbH in Duisburg, Germany and a good agreement is found. In terms of numerical analysis, computational times, solution procedures and the model's overall convergence behaviour are briefly discussed.

Keywords: High-temperature polymer-electrolyte-membrane (HTPEM) fuel cell, Fuel cell modeling, Polybenzimidazole (PBI), Phosphoric acid (H_3PO_4), Membrane behaviour.

1. Introduction

Polymer-electrolyte-membrane (PEM) fuel cells are expected to play a key role in forthcoming power-delivering devices. Beside the well known advantages of the low temperature PEM there are some major drawbacks that are directly related to the operating conditions (e.g., 80°C, high gas humidification). Consequently, much attention has been paid to high-temperature polymer-electrolyte-membrane (HTPEM) fuel cells. Phosphoric acid (H_3PO_4) doped polybenzimidazole (PBI) membranes have been investigated over the last decade and are commonly used in today's HTPEM technology in order to achieve the requested high proton conductivity [1].

Much modeling and simulation work has been published for low-temperature PEM fuel cells but only a few computational fluid dynamics studies are currently available in literature covering HTPEM fuel cells. Cheddie and Munroe [1-3] published several studies accounting for various operating conditions and layouts. These models were solved using COMSOL Multiphysics in one-, two, and three-dimensions. Peng et al. [4,5] presented three-dimensional, steady-state and transient studies using control volumes. Our group recently published a two-dimensional study with an emphasis on overall quantities behaviour [6]. The sol-gel PBI/H_3PO_4 membrane was modeled using an empirical relationship. Moreover, a two-equation energy conservation was introduced to specifically locate hot-spots. Experimental data was compared with simulation results and a good agreement was found.

In this study, the former developed two-dimensional model is extended to the third dimension to get a more realistic view of the internal quantities and membrane behaviour at different operating points. Cell optimization potential is shortly discussed. Further, solution procedures and convergence behaviour for different implemented solvers are highlighted.

2. HTPEM model set-up

2.1 Computational domain

Fig.1 shows the computational domain as well as the used computational mesh. It consists of two single gas channels to continuously feed the air and hydrogen in counterflow configuration. The channels are machined into our in-house, high-temperature stable, highly conductive (electrical and thermal) bipolar plates

(polyphenylene sulfide (PPS) based). The total thickness of a pristine, uncompressed high temperature membrane electrode assembly (MEA) is expected to be 900-1000·10^{-6} [m]. In our model, the 5-layer MEA consists of two gas diffusion layers (GDL – light grey – ±320·10^{-6} [m]) to equally distribute the incoming gases over the entire reaction layer surface. Within both reaction layers (RL – black – ±50·10^{-6} [m]), the well known electrochemical half-cell reactions take place.

$$2 \cdot H_2 \rightarrow 4 \cdot H^+ + 4 \cdot e^- \quad (1)$$

$$O_2 + 4 \cdot H^+ + 4 \cdot e^- \rightarrow 2 \cdot H_2O_{v,l} \quad (2)$$

The sol-gel PBI/H_3PO_4 membrane (orange – ±100·10^{-6} [m]) separates the anode from the cathode side and transports protons via the Grotthuss proton switching mechanism [9].

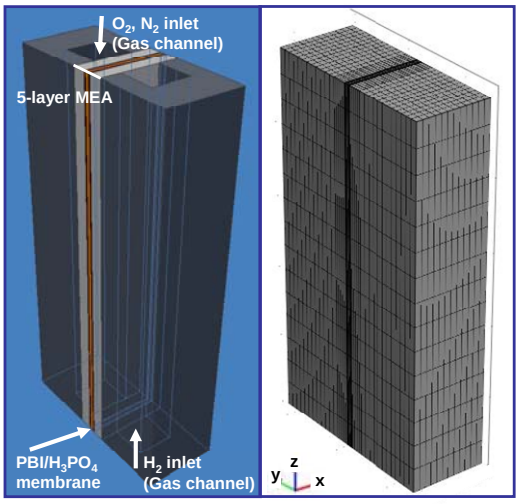

Figure 1. Left: Computational domain including gas channels, bipolar-plates, and the 5-layer MEA; Right: Structured mesh

2.2 Assumptions

The following assumptions are used in this model: i) steady-state operating conditions, ii) single-phase water flow since the fuel cell operates at higher temperatures, iii) laminar gas flow within all gas channels, iv) fully developed gas inlet conditions, v) all gases are treated as ideal, vi) all electrochemical reactions are gaseous phase reactions, vii) no crossover of gases through the membrane, viii) all material parameters are isotropic and homogeneous, ix) the PBI/H_3PO_4 membrane is considered as a system of PBI, H_3PO_4 and H_2O only (other forms of acid are neglected), x) the initial amorphous phase H_3PO_4 concentration is 80-85 [wt.%], xi) no interaction between the water and the amorphous phase H_3PO_4, and xii) no water transfer through the membrane.

2.3 Governing equations - Subdomains

COMSOL Multiphysics is used to solve this complex HTPEM fuel cell model. The conservation equations are solved sequentially (and grouped) for the variables velocity vector u [m·s^{-1}], pressure P [Pa], species mass/mole fraction ω_i [-], electrical ϕ_s [V] and protonic phase potential ϕ_m [V], and solid T_s [K] and fluid-(gas)-phase temperature T_f [K]. All conservation equations are strictly used in their conservative form and are very similar to the ones given in [6].

The incompressible Navier-Stokes application mode is used to describe the gas flow through the channels (3)

$$\begin{gathered} \nabla \cdot u = 0 \\ \rho \cdot u \cdot \nabla u = \\ \nabla \cdot \left(-P \cdot I + \eta \cdot \left(\nabla u + (\nabla u)^T \right) \right) \\ + F \end{gathered} \quad (3)$$

and through the porous media (Brinkman equations) (4).

$$\begin{gathered} \nabla \cdot u = 0 \\ \frac{\eta}{k_{p,i}} \cdot u = \\ \nabla \cdot \left(-P \cdot I + \frac{1}{\varepsilon_i} \cdot \eta \cdot \left(\nabla u + (\nabla u)^T \right) \right) \\ + F \end{gathered} \quad (4)$$

In (3) and (4), ρ is the density [kg·m^{-3}], η the dynamic viscosity [Pa·s^{-1}], $k_{p,i}$ [m^2] the permeability, and ε_i [-] the porosity of the porous media.

The governing equations for species (Maxwell-Stefan diffusion and convection application

mode), charge (conductive media DC application mode), and energy conservation (conduction and convection respectively conduction application mode) are the same as in [6], extended to the third dimension and are not repeated herein. Moreover, all source term couplings are identically to the ones in [6].

2.4 PBI/H_3PO_4 membrane considerations

A highly doped sol-gel PBI/H_3PO_4 membrane of approximately 30-35 mol of H_3PO_4 per PBI repeat unit finally consists of more than ±85 [wt.%] H_3PO_4 [7]. Since two H_3PO_4 molecules are bonded to PBI (crystalline region), *X*-2 molecules remain free and tend to form an amorphous phase within the sol-gel PBI/H_3PO_4 matrix.

In this model, the amorphous phase volume fraction is calculated based on densities [3].

$$V_{H_3PO_4} = \left(\frac{4.81}{X-2} + 1 \right)^{-1} \tag{5}$$

Fig.2 represents $V_{H_3PO_4}$ [Vol.%] as a function of the membrane doping level *X* [-], showing a saturation behaviour at very high doping levels.

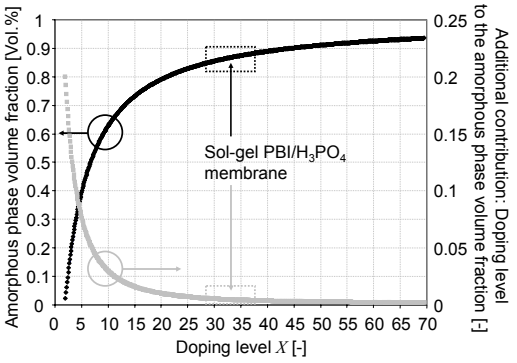

Figure 2. Amorphous phase volume fraction for different membrane doping levels; Additional contribution: Doping level to the amorphous phase volume fraction

It is widely accepted that the free (amorphous phase) H_3PO_4 mainly contributes to high membrane conductivity via a Grotthuss proton switching mechanism [8,9]. Moreover, the strong temperature dependency of the membrane conductivity can accurately be described using an Arrhenius approach (6) [8,9].

$$\sigma = \frac{\sigma_0(k_i, X)}{T_s} \cdot e^{\left(-\frac{\Delta E(k_i, X)}{R \cdot T_s} \right)} \tag{6}$$

The pre-exponential term σ_0 [S·K·m^{-1}] is assumed to be independent from cell operating temperature and decreases with higher doping levels *X* [7]. In (7), *C* [mol·m^{-3}] is the concentration of the mobile species. Among others, the concentration changes with *X* and σ_0 is expected to reach the value of concentrated H_3PO_4 [7].

$$\sigma_0 = \left(\frac{z^2 \cdot F^2}{R} \right) \cdot \alpha \cdot \upsilon_0 \cdot d^2 \cdot C \cdot e^{\frac{\Delta S + \Delta S_f}{R}} \tag{7}$$

The activation energy ΔE [J·mol^{-1}] is also expressed in terms of *X* and is the sum of the enthalpies $\Delta H + \Delta H_f$. Only minor valuable data are available in open literature for sol-gel membranes [9-12]. Consequently, both terms (σ_0 and ΔE) are empirically correlated to the values of concentrated H_3PO_4 (85 [wt.%]) (see Fig.3 – $V_{H_3PO_4}$ = 1) and described using the following equation.

$$\sigma_0, \Delta E = k_1 \cdot \ln(X) + k_2 \tag{8}$$

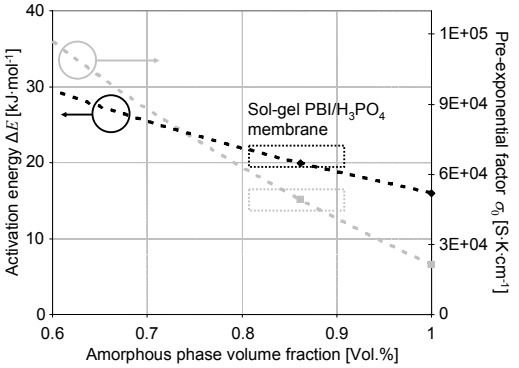

Figure 3. Empirically correlated values for activation energy; Pre-exponential factor for different membrane doping levels

2.5 Porous media considerations and physical-chemical properties

This model considers a woven-type GDL (e.g., E-tek - ELAT®) with an assumed porosity of 0.7 [-] (uncompressed). The RL consists of i) a GDL weight fraction ii) a carbon black/platinum weight fraction of 30 [wt.%] (e.g., Vulcan XC-72), and iii) a PBI/H_3PO_4 weight fraction of 30 [wt.%]. The anode RL platinum loading is supposed to be 0.01 [kg·m^{-2}] and the cathode RL loading 0.0075 [kg·m^{-2}]. The calculated weight fractions are used to correlate e.g., the electrical/protonic conductivities and the diffusion coefficients of porous media using a Bruggemann correlation.

Similar to [6], the reaction layer permeability is calculated taking a packed bed of spherical particles into account. Further, all material and gas properties are carefully declared with respect to the higher operating temperatures.

2.6 Governing equations – Boundary conditions

All boundary and initial conditions are carefully defined according to the experimental set-up. Gas composition, temperature (fluid-(gas)-phase), and velocity are declared at the gas channel inlets. At the outlets, pressure and convective flux boundary conditions are used. The cell operating temperature (solid-phase) and cell voltage are defined at the bipolar plate boundaries. At internal boundaries, symmetry, continuity or thermal insulation boundary conditions are used.

3. Computational techniques

The dimensions of the geometry were 0.002 [m] x 0.004915 [m] x 0.01 [m]. A structured mesh was used for all computations and consisted of 8,820 hexahedral elements. The minimum element quality was 0.0178 (element volume ratio 0.06). The gas channel was discretization using 6 x 6 x 15 elements. The GDL, RL, and PBI/H_3PO_4 membrane subdomains were discretized using 5 elements in *y*-direction (see Fig.1).

This highly coupled system of partial differential equations was solved sequentially using solver scripting while using the computed results as initial guesses within the next solution step. The charge conservation was solved first. In a second step, the mass/momentum conservation was solved. Finally, the energy conservation was solved while iteratively updating previous results.

Depending on the cell voltage, calculations were performed using the PARDISO direct solver (±8,400 seconds for base case operating conditions) or the segregated group solver (group 1: P, u; group 2: ω_i; group 3: ϕ_s , ϕ_m , T_s, T_f) (±4,850 seconds for base case operating conditions) on an 8GB RAM, Quad-Core machine (64-Bit). The total number of degrees of freedom was roughly 400,000. The convergence criterion was set to $1 \cdot 10^{-3}$ – $1 \cdot 10^{-6}$.

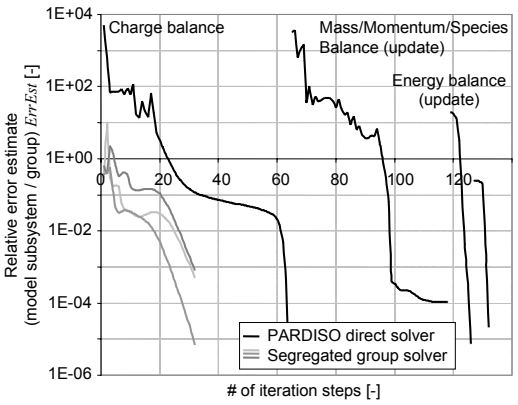

Figure 4. Model subsystem / group convergence behaviour over the number of iteration for base case operating conditions at U_{cell} = 0.6 [V]: PARDISO solver – black, Segregated group solver – grey)

4. Simulation results

Fig.5 shows the oxygen mass fraction at different internal subdomains boundaries within the cell. The cell voltage is 0.6 [V]. The mass fraction is higher under the gas channel than under the both current collectors and is continuously consumed in *z*-direction due to electrochemical reactions.

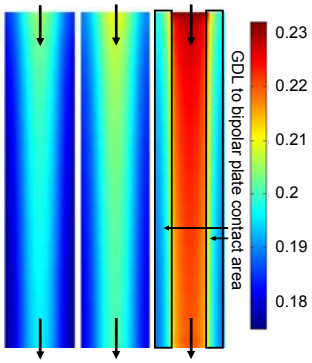

Figure 5. Oxygen mass fraction [-] at the internal boundaries PBI/H_3PO_4 – RL (left); RL – GDL (middle); GDL – bipolar plate (right)

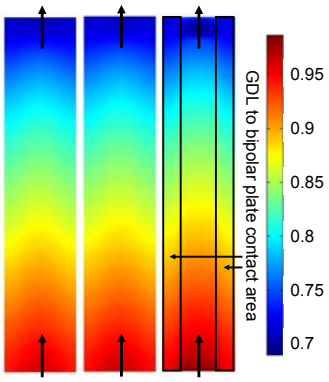

Figure 6. Hydrogen mass fraction [-] at the internal boundaries PBI/H_3PO_4 – RL (left); RL – GDL (middle); GDL – bipolar plate (right)

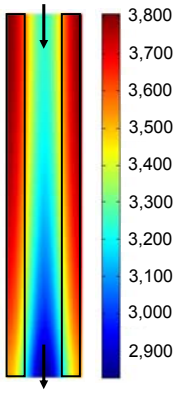

Figure 7. Average cathode side RL current density [A·m^{-2}] (U_{cell} = 0.6 [V])

The anode side H_2 mass fraction distribution is much smoother, showing small gradients in *x*-, and *z*-direction. It is proposed that hydrogen easily reaches electrochemical active sites.

The average cathode side RL current density is shown in Fig.7. The distribution is mainly dependent on the species mass fractions and the local overpotentials. Consequently highest values are located under the bipolar plate, possibly due to ohmic losses.

Fig.8 shows the distribution of the solid- and fluid-(gas)-phase temperatures. In [6] it has already been noticed that a severe influence between both variables exists, especially when entering the cell at low gas temperatures. The solid-phase heat flux vectors indicate the heating of the cell, keeping it at 160°C. The fluid-(gas)-phase heat flux vectors show that heat is slightly absorbed form the solid-phase (e.g., GDL solid structure) by the gas streams. Consequently, the temperature of both gases slightly rises along the channel length. In this model set-up, T_s equals T_f within the RL.

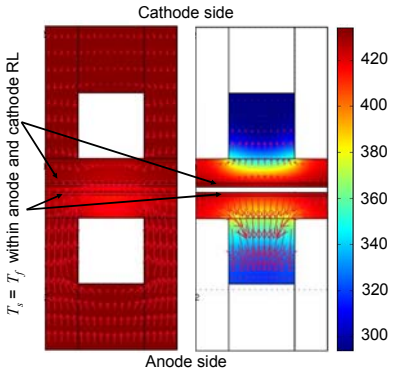

Figure 8. Solid-phase temperature and heat flux vectors (left); Fluid-(gas)-phase temperature and heat flux vectors (right) (U_{cell} = 0.6 [V]) (Slice plot at z/z_{max} = 0.25)

The sol-gel PBI/H_3PO_4 membrane conductivity distribution is given in Fig.9. The cold gases entering the cell may cool the cell at local spots, leading to lower proton conductivity values implying higher ohmic (protonic) losses over the membrane, again influencing the local current density distribution. The average values are slightly under 22 [S·m^{-1}] (T_s = 160°C) and 25 [S·m^{-1}] (T_s = 170°C) which is comparable to the values given in [7]. Comparing these values with the conductivity values of H_3PO_4 [10] for similar

conditions (160°C – 80 [wt.%] → ±65 [S·m^{-1}] and 170°C – 80 [wt.%] → ±69 [S·m^{-1}])) returns a ratio of ±0.3 [-], indicating that the transport process through the sol-gel PBI/H_3PO_4 membrane is possibly not as continuous as in H_3PO_4, even at high doping levels.

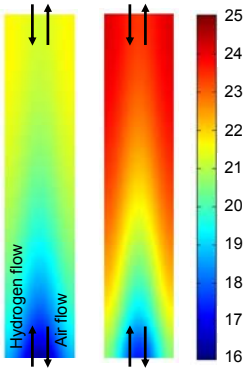

Figure 9. Sol-gel PBI/H_3PO_4 membrane conductivity distribution for 160°C (left) and 170°C (right) (U_{cell} = 0.6 [V])

The voltage losses over the membrane are calculated using the membrane thickness l_m [m] and the following equation

$$U_{\Omega,mem} = \frac{i_m}{\sigma_m} \cdot l_m \qquad (15)$$

The IV-curve in Fig.12 is mainly dominated by activation and ohmic losses. For 160°C, the calculated ohmic voltage losses returned ±0.04 [V] at U_{cell} = 0.6 [V].

5. Experimental investigations

The Zentrum für BrennstoffzellenTechnik (ZBT) gGmbH in Duisburg, Germany, is working for several years in the field of HTPEM fuel cell research and development. Consequently, all tests were run at their facilities under precisely defined operating conditions (see Fig.10).

The base case cell operating temperature was controlled at 160°C using a heated aluminum end-plate. Gases (H_2 – ±0.25% relative humidity, air – ±4% relative humidity) were feed at room temperature using stoichiometric flow rates of 1.35 [-] (H_2) and 2.5 [-] (air) (ambient pressure at both outlets).

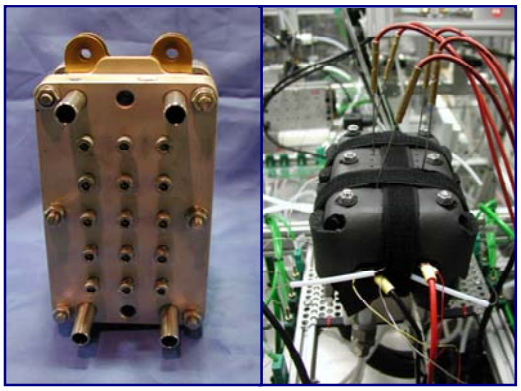

Figure 10. Left: Specially designed HTPEM fuel cell; Right: Cell during operation at ZBT

Fig.11 compares the simulated at measured IV- and power density curves. It should be noted that the exchange current density i_0 [A·m^{-2}] is used as a tuning parameter within a reasonable range given in [12].

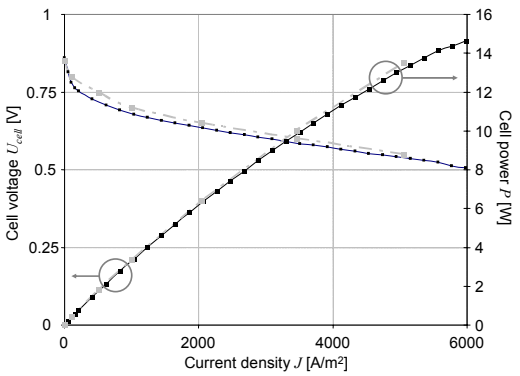

Figure 11. Measured (black) and simulated (grey) IV- and power curves for a HTPEM fuel cell (T_s = 160°C, T_f = 21°C)

6. Conclusions

This work presented a complete three-dimensional HTPEM fuel cell models using a sol-gel PBI/H_3PO_4 membrane. Most material parameters were based on the latest publications in the field and from data sheets. It was shown, that the cathode side flow-field layout is one major optimization parameter in order to increase and equally distribute the oxygen near

the RL. Further, the gas-(fluid)-phase temperature should be considered as an important operating parameter for cell tempering. Overall a good agreement was found between the measured and simulated results. Many more investigations are necessary to precisely validate the model set-up. Including gas solubility at electrochemical active sites is a task for future work. The model will more accurately describe the mass limitation effects by taking the amount of H_3PO_4 within the RL into account.

7. References

1. Cheddie, D., Munroe, N., Parametric model of an intermediate temperature PEMFC, *J. Power Sources*, **156**, 414-423 (2006)
2. Cheddie, D., Munroe, N., Three dimensional modeling of high temperature PEM fuel cells, *J. Power Sources*, **160**, 215-223 (2006)
3. Cheddie, D., Munroe, N., A two-phase model of an intermediate temperature PEM fuel cell, *Int. J. Hydrogen Energy*, **32**, 832-841 (2007)
4. Peng, J., Lee, S.J., Numerical simulation of proton exchange membrane fuel cells at high operating temperature, *J. Power Sources*, **162**, 1182-1191 (2006)
5. Peng, J., Shin, J.Y., Song, T.W., Transient response of high temperature PEM fuel cell, *J. Power Sources*, **179**, 220-231 (2008)
6. Siegel, C., Bandlamudi G., Heinzel, A., *Proceedings of the European COMSOL Conference – Vol. 1 Numerical simulation of a high-temperature PEM (HTPEM) fuel cell*, 428-434, Petit, J.-M., Squalli, O., Grenoble, France (2007)
7. Xiao, L., Zhang, H., Scanlon, E., Ramanathan, S., Choe, E.-W., Rogers, D., Apple, T., Benicewicz, B.C., High-temperature polybenzimidazole fuel cell membranes via a sol-gel process, *Chem. Mater.*, **17**, 5328-5333, (2005)
8. Zhang, J., Xie, Z., Zhang, J., Tang, Y., Song, C., Navessin, T., Shi, Z., Song, D., Wang, H., Wilkinson, D.P., Liu, Z.-S., Holdcroft, S., High temperature PEM fuel cells, *J. Power Sources*, **160**, 872-891 (2006)
9. Ma, Y.-L., The fundamental studies of polybenzimidazole/phosphoric acid polymer electrolyte for fuel cells, Dissertation, Case Western Reserve University, U.S.A. (2004)
10. Chin, D.-T., Chang, H.H., On the conductivity of phosphoric acid electrolyte, *J. Appl. Electrochem.*, **19**, 95-99 (1989)
11. Bouchet, R., Siebert, E., Proton conduction in acid doped polybenzimidazole, *Solid State Ionics*, **118**, 287-299 (1999)
12. Zhang, J., Tang, Y., Song, C., Zhang, J., Polybenzimidazole-membrane-based PEM fuel cell in the temperature range of 120-200°C, *J. Power Sources*, **172**, 163-171 (2007)

8. Acknowledgements

This work was supported by 'LE GOUVERNEMENT DU GRAND-DUCHÉ DE LUXEMBOURG, MCESR – Recherche et Innovation', Grant No.: BFR07/007.